Observed interannual relationship between ITCZ position and tropical cyclone frequency

Article

Accepted Version

Observed interannual relationship between ITCZ position and tropical cyclone frequency

Xiaoqing Liao,[a,b] Christopher E. Holloway,[c] Xiangbo Feng,[c,d] Chunlei Liu,[*a,c] Xinyu Lyu,[e] Yufeng Xue, [*a,b] Ruijuan Bao,[f] Jiandong Li,[g] Fangli Qiao,[h]

[a] *South China Sea Institute of Marine Meteorology, Guangdong Ocean University, Zhanjiang, China*

[b] *College of Ocean and Meteorology, Guangdong Ocean University, Zhanjiang, China*

[c] *Department of Meteorology, University of Reading, Reading, UK*

[d] *National Centre for Atmospheric Science, University of Reading, Reading, UK*

[e] *Tianjin Jizhou Meteorological Bureau, Tianjin, China*

[f] *Fujian Key Laboratory of Severe Weather, Fuzhou, China*

[g] *Institute of Atmospheric Physics, Chinese Academy of Sciences, Beijing, China*

[h] *First Institute of Oceanography, and Key Laboratory of Marine Science and Numerical Modeling, Ministry of Natural Resources, Qingdao, China*

Corresponding author: Chunlei Liu, liuclei@gdou.edu.cn

Yufeng Xue, xueyf@gdou.edu.cn

ABSTRACT

There are no well accepted mechanisms that can explain the annual frequency of tropical cyclones (TCs) both globally and in individual ocean basins. Recent studies using idealized models showed that the climatological frequency of TC genesis (TCG) is proportional to the Coriolis parameter associated with the intertropical convergence zone (ITCZ) position. In this study, we investigate the effect of the ITCZ position on TCG on the interannual time scale using observations over 1979-2020. Our results show that the TCG frequency is significantly correlated with the ITCZ position in the North Atlantic (NA) and Western North Pacific (WNP), with more TCG events in years when the ITCZ is further poleward. The ITCZ-TCG relationship in NA is dominated by TCG events in the tropics (0-20°N), while the relationship in WNP is due to TCs formed in the east sector (140-180°E). We further confirmed that the ENSO has little effect on the ITCZ-TCG relationship despite it can affects the ITCZ position and TCG frequency separately.

In NA and WNP, a poleward shift of ITCZ is significantly associated with large-scale environment changes favoring TCG in the Main Development Region (MDR), However, the basin-wide TCG frequency has a weak relationship with the ITCZ in other ocean basins. We showed that a poleward ITCZ in Eastern North Pacific and South Pacific favors TCG on the poleward flank of MDR, whilst it suppresses TCG on the equatorward flank, leading to insignificant change in basin-wide TCG frequency. In the South Indian Ocean, the ITCZ position has weak effect on TCG frequency due to mixed influences of environmental conditions.

1. Introduction

Although many studies have been carried out, there are still no well accepted mechanisms that can explain the annual frequency tropical cyclones (TCs) globally and in individual ocean basins. From year to year, the global TC frequency is about 90 which is relatively stable (Emanuel 1991, 2006), it could be dynamically constrained by the maximum TC disturbances associated with the ITCZ (Intertropical Convergence Zone) breakdown at any instant time under current tropical atmospheric conditions (Wang et al. 2019). The ITCZ can provide sufficient background vorticity and moisture (Kieu and Zhang 2008; Vu et al. 2021) and a disturbance caused by ITCZ breakdown could trigger the TCG (TC genesis) (Ferreira and Schubert 1997; Wang and Magnusdottir 2006; Kieu and Zhang 2008; Yokota et al. 2015; Wang et al. 2019). The basin-wide frequency varies greatly in observations. There are differences in TCG annual frequency and seasonal variations between basins in model simulations (Sobel et al. 2021), and it is difficult for the observed annual TCG frequency to be represented accurately in simulations (Hoogewind et al. 2020). Further studies are needed to understand the role of ITCZ position in determining the annual frequency of TCs globally and in individual basins (Hoogewind et al. 2020; Sobel et al. 2021).

Previous studies have focused on the ITCZ-TCG relationship using idealized aquaplanet simulations and the Coriolis effect has been examined (Merlis et al. 2013; Ballinger et al. 2015; Merlis and Held 2019; Burnett et al. 2021). Hsieh et al. (2020) showed that there are more TCG events when the ITCZ moves poleward, likely related to both the increase of synoptic precursors and the probability of developing into TC because of the reduced wind shear and increased Coriolis parameter. Merlis et al. (2013) indicated a 40% increase in the TCG frequency per degree poleward shift of the ITCZ location when the radiative forcing is unchanged. Similar idealized simulations were also carried out by Ballinger et al. (2015), who found a climatological increase of TC frequency when the maximum sea surface temperature (SST) shifts poleward, and when the tropical meridional SST gradient increases. Ballinger et al. (2015) showed that both the ITCZ and genesis locations shift poleward when the maximum SST moves poleward. Burnett et al. (2021) also showed an overall increase of the TC frequency in idealized models when the maximum SSTs and ITCZ move poleward, and found that the TCG frequency is proportional to the Coriolis parameter at the ITCZ location, i.e., when the ITCZ shifts poleward, the TCG frequency increases. When applied to observations, this ITCZ-TCG relationship generally captures the seasonal cycle of TC

frequency well across most TC basins (Burnett et al. 2021). It was hypothesized that the ITCZ-TCG relationship is due to the higher cyclonic vorticity at the poleward flank of the ITCZ (Ballinger et al. 2015). When the ITCZ moves poleward, the local planetary vorticity felt by precursor disturbances associated with the ITCZ will be enhanced, leading to a higher likelihood of cyclogenesis. The Coriolis parameter *f* at the ITCZ is considered to be the key factor controlling these precursor disturbances (Burnett et al. 2021). The TCG increases almost linearly with *f* in the tropical region (Chavas and Reed 2019).

These studies concentrated on the correlation between TC frequency and the ITCZ position in idealized model configurations which avoids the complexity caused e.g., by the asymmetry of continents (Merlis et al. 2013; Ballinger et al. 2015; Burnett et al. 2021). On the one hand, both TC formation and the ITCZ have their own unique characteristics over different basins. On the other hand, the TCG development is also restrained by other large-scale environmental conditions, such as the SST, moisture in the middle troposphere, vertical wind shear, and absolute vorticity in the lower troposphere (Palmen 1948; Gray 1968, 1979; Ritchie and Holland 1997; DeMaria et al. 2001; Cheung 2004; Dowdy et al. 2012; Hoogewind et al. 2020). In the real world, these environmental factors could compete with each other, together with the ITCZ effect, modulating the TCG occurrence by affecting the precursors and their survival rate to TCG (Ikehata and Satoh 2021). Further studies are needed to understand what roles are played by these environmental factors in the TCG occurrence when the ITCZ shifts poleward or equatorward. The co-variability of TCG frequency and the ITCZ position on seasonal timescales makes difficult to further interpret the underpinning processes in the ITCZ-TCG relationship. It is not known whether the ITCZ-TCG relationship initially proposed for seasonal timescales will be useful to understand the interannual variability of TCG event.

The ENSO (El Niño-Southern Oscillation) can affect both ITCZ and TCG since they significantly influence the large scale atmospheric and oceanic conditions (Ramsay et al. 2012; Adam et al. 2016a, 2016b; Zhao and Wang 2019; Feng et al. 2020a, b; Schmitt et al. 2020; Kim and Moon 2022). In this study, we will address the following science questions: (1) What is the interannual relationship in observations between the ITCZ location and the TCG frequency globally and in different ocean basins with and without ENSO influences? and (2) What roles are played by environmental conditions in this relationship? The data and methods will be introduced in Section 2. Section 3 will present the observed relationship

between TCG frequency and the ITCZ position in each basin and hemisphere, followed by interpretation of the relationship by employing large-scale environmental factors. Section 4 will present the summary and discussion.

2. Data and methods

a. Data

The IBTrACS (International Best Track Archive for Climate Stewardship) version 4 dataset (Knapp et al. 2010, 2018) from 1979 to 2020 is used to calculate TCG frequency and location in the satellite era. IBTrACS data are TC Best Track observations, containing the maximum sustained wind speed, minimum sea level pressure and location at 6-hourly intervals. Best Track observations used in this study are from USA agencies, such as the National Hurricane Center (NHC), Joint Typhoon Warning Center (JTWC) and Central Pacific Hurricane Center (CPHC). In our study, we only include TCs whose maximum sustained wind speed $U_{max} \geqslant 33$ knots, and the first track point reaching 33 knots is defined as the TCG location.

The monthly ITCZ location and intensity is calculated from the monthly GPCP (Global Precipitation Climatology Project) version 2.3 data (Adler et al. 2003, 2018), at the spatial resolution of 2.5˚×2.5˚. The GPCP data combine data from various sources including satellite products, gauge measurements and sounding observations.

b. ITCZ position and intensity

To mitigate the effect of the low resolution in precipitation data on the ITCZ identification, a centroid method is used following Frierson and Hwang (2012), Donohoe et al. (2013) and Burnett et al. (2021). The ITCZ positions in northern (θ_{NH}) and southern (θ_{SH}) hemispheres can be defined as:

$$\theta_{NH} = \frac{\int_0^{20} \varphi \times p \times cos\varphi d\varphi}{\int_0^{20} p \times cos\varphi d\varphi} \quad (1)$$

$$\theta_{SH} = \frac{\int_{-20}^{0} \varphi \times p \times cos\varphi d\varphi}{\int_{-20}^{0} p \times cos\varphi d\varphi} \quad (2)$$

where φ is the latitude (°) and p the precipitation (mm/day). The integral is from 0° to 20°N for NH basins and from 20°S to 0° for SH basins. The corresponding ITCZ intensity is defined as the mean precipitation of the two latitudes that are closest to the ITCZ position.

Both the ITCZ position and intensity are calculated at each longitude first and then averaged over the longitude range of each basin (see next subsection). Both land and ocean grid points in the defined area are included in the calculation.

Considering the uncertainty of the ITCZ position from different definitions and datasets, the maximum precipitation method (Liu et al. 2020) is also employed to compare with the centroid method, and the corresponding ITCZ precipitation is the longitudinal mean at the ITCZ latitude. Other datasets with different spatial resolutions, including the ERA5 (0.25˚×0.25˚), TRMM (Tropical Rainfall Measuring Mission, 0.25˚×0.25˚, Huffman et al. 2007) and GPCP (1.0˚×1.0˚), are also used to check the robustness of our results.

c. TCG and ITCZ regions

As defined in IBTrACS, we have six ocean basins for TCG, which are the North Atlantic (NA), Western North Pacific (WNP), Eastern North Pacific (ENP) and North Indian Ocean (NIO) in the Northern Hemisphere (NH), and South Indian Ocean (SIO) and South Pacific (SP) in the Southern Hemisphere (SH) (Figures 1 and S1-S6). Since there are only three observed TCs in the South Atlantic over 1979-2020 (Figure 1a), it is excluded from this study.

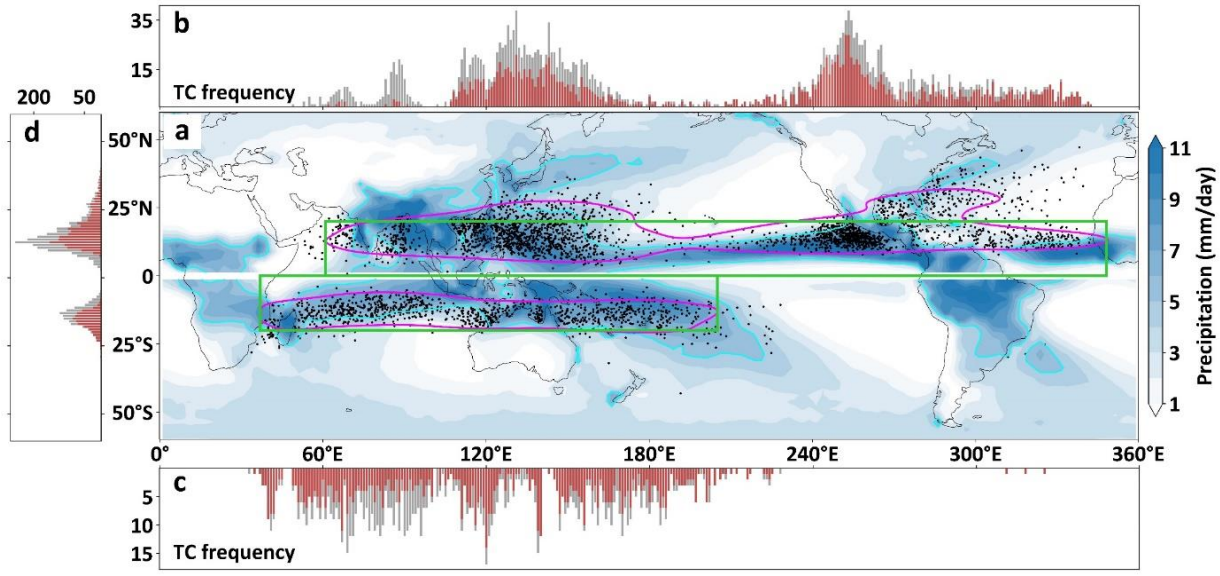

Figure 1. (a) TCG locations (black dots) and TC season mean precipitation (shaded) in the NH and SH over 1979-2020. Cyan contours represent the climatological rainfall of 5 mm/day. Magenta contours are areas accounting for at least 80% of the number of TCG using Kernel Density Estimation. The green boxes represent the area boundaries for ITCZ location calculation in NH and SH, with the same longitude ranges as the magenta contours. The green box range is (61°-348°E, 0°-20°N) in NH and (37°-205°E, 0°-20°S) in SH. The TC season is JAS in NH and JFM in SH. (b) Red bars represent total TC numbers at 1° longitude

interval in NH TC season over 1979-2020, while grey bars represent those in the whole year. (c) As (b), but for SH. (d) As (b) and (c), but for TC numbers at 1° latitude interval. The configurations for basin-wide TCG and ITCZ definitions are provided in Table S1 and Figures S1-S6 in supplementary material. The abbreviated basin names are also listed in Table S1.

The ITCZ in the main TCG region is used to study the ITCZ-TCG relationship. The main TCG region is estimated for each ocean basin and each hemisphere (Figures 1 and S1-S6) using Kernel Density Estimation (KDE) (Ivezić et al. 2019; Zhao et al. 2015; Zhao et al. 2021). The magenta contour (Figures 1 and S1-S6) is calculated from KDE and contains 80% of TCG events over the target basin (Figures 1 and S1-S6). The boundaries of the magenta contour are used to define the longitudinal range (green boxes in Figures 1 and S1-S6) for the calculation of the ITCZ position, except in NA and SP where the green box ends at the west coast of the ocean basin. The latitude ranges for the ITCZ calculation are 0-20°N in NH and 0-20°S in SH. The TCG event is counted in each target basin defined by IBTrACS. The boundary ranges for each basin, ITCZ calculations, and abbreviated basin names are shown in Table S1.

The TC season is defined to be from July to September (JAS) for basins in the NH and from January to March (JFM) for basins in SH. The whole year is defined to be from January to December in NH and from July to June in SH. The number of TCG in TC seasons is about 57.1% of the total occurrence in NH and about 63.4% in SH over 1979-2020 (Figure 1).

As expected, there is a clear co-variation between the ITCZ position and TCG frequency on monthly scale in individual ocean basins and hemispheres (Figure S7), except for the NIO where the TCG frequency has two peaks due to the strong vertical wind shear during the monsoon period (Gray 1968; Li et al. 2013; Swapna et al. 2022). The ITCZ location is generally the most poleward in the peak season of TCG (Liu et al. 2020). Unless otherwise stated in this study, the ITCZ position in a basin will be the mean latitude of the ITCZ region in the TC season, and the TCG frequency will be the total number of TCG events in the TC season. The NIO will be excluded in the following analysis because there are too few TCs during the period from July to September.

d. Removal of the linear signal associated with ENSO

Many studies have shown the ENSO influences on the ITCZ position and TC frequency, since it could not only modulate the meridional SST gradient, affect trade winds and lead to

the regional ITCZ migration (Bischoff and Schneider 2014; Schneider et al. 2014; Sasaki et al. 2015; Fu et al. 2017; Zhao et al. 2021), but also modulate the large-scale circulation, change environmental conditions such as the wind shear, vertical motion and adjust TC activities. In this study, the ITCZ-TCG relationship is compared before and after removing the ENSO effect from ITCZ position and TCG frequency.

The Oceanic Niño Index (ONI) from NOAA (National Oceanic and Atmospheric Administration) is an ENSO indicator which is the three-month running mean of SST anomaly over the Niño 3.4 region (5°N-5°S, 120°-170°W). The El Niño years and La Niña years are defined such that there is a minimum of 5 consecutive overlapping seasons including the TC season with ONI≥0.5℃ (El Niño year) or ONI≤0.5℃ (La Niña year), which are listed in Tables S2 and S3 for NH and SH, respectively. A linear model $y = m \times \mathrm{ONI} + a$ (where m and a are constants) is regressed to estimate the linear effect of ENSO on the ITCZ position or TCG frequency. The ENSO effect could be excluded by only using the neutral years, or subtracting the regressed model from the ITCZ and TC frequency timeseries (Feng et al. 2021). The second method is used in this study.

e. Statistical analysis methods

The Wald test with t-distribution is used for the significance test of the regression slope and the two-tailed t-test is used for the significance test of the Pearson correlation coefficient (Wilks 2011) in this study. The time series of the ITCZ position, TCG frequency and TCG location have been detrended, in order to focus on the interannual variability of their relationships.

f. Environmental conditions

The environmental variables, such as the SST, relative humidity (RH) at 600 hPa, vertical wind shear (WS) between 200 and 850 hPa, and the relative vorticity (RV) at 850 hPa, are important factors affecting the TCG. Their changes and influences on the TCG are investigated in this study. In order to evaluate the integrated effect of environment factors on TCG, the GPI (genesis potential index) is also calculated based on Emanuel and Nolan (2004)

$$GPI = |10^5\eta|^{3/2}\left(\frac{RH}{50}\right)^3\left(\frac{V_{pot}}{70}\right)^3(1+0.1WS)^{-2} \quad (3)$$

where η is the absolute vorticity at 850 hPa (s^{-1}), which is the Coriolis parameter plus the

relative vorticity. V_{pot} is the potential intensity (m s^{-1}, Emanuel 1986). All of these variables are downloaded or calculated from the ERA5 monthly reanalysis (Hersbach et al. 2020), with horizontal resolution of 0.25°×0.25°.

3. Results

a. Interannual relationship between ITCZ position and TCG frequency

The relationship between the ITCZ position and TCG frequency over different basins and hemispheres is shown in Figure 2. The regressions and correlations (magenta line and number) are generally positive in the NH basins (left column) and negative in SH (right column), implying the increase of the TCG frequency when the ITCZ shifts poleward. Significant correlations (correlation coefficient *r* in bold) are only found in NH basins, with *r* ⩾0.41 in

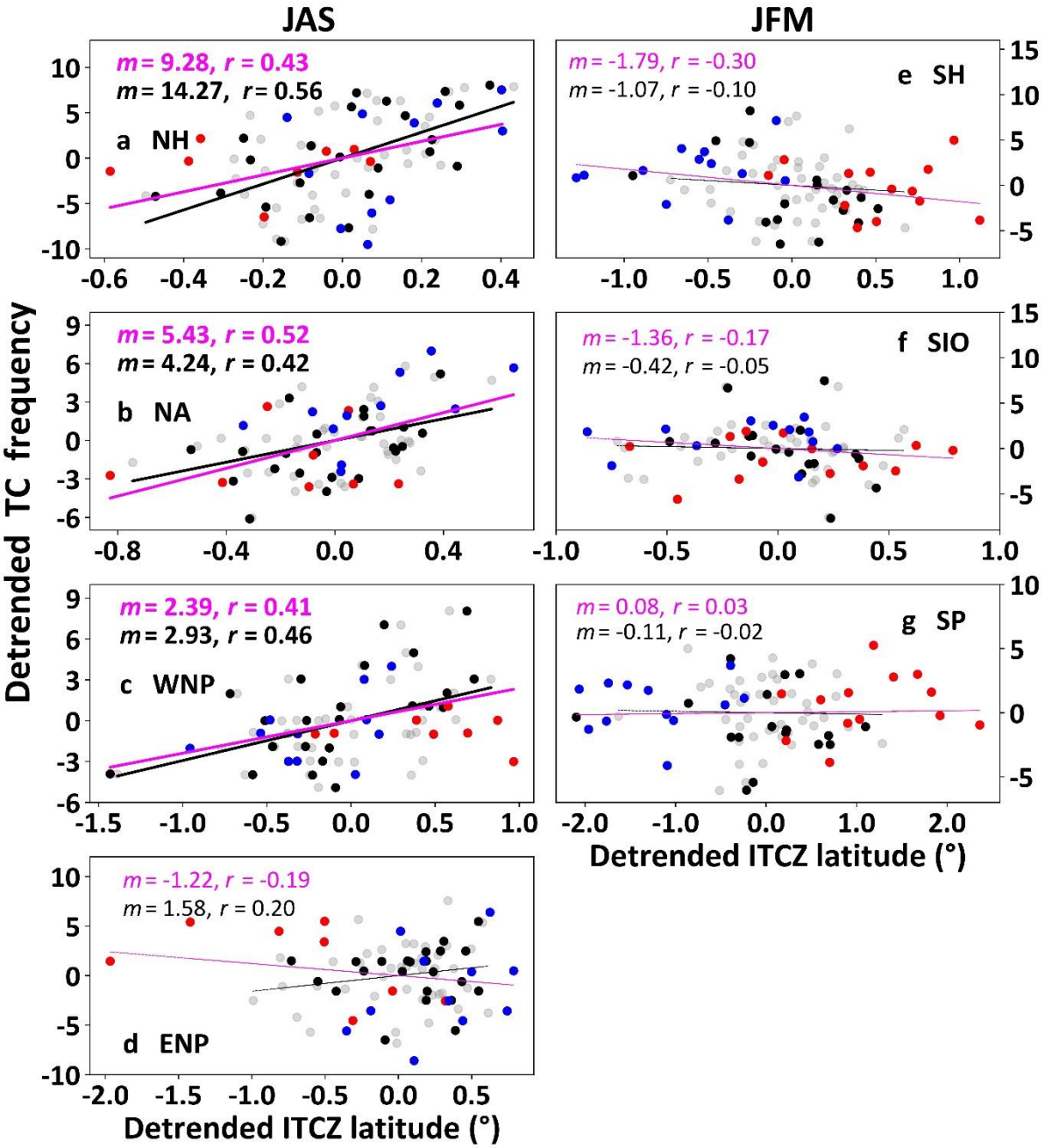

231

232 Figure 2. Scatter plot between the detrended values of ITCZ latitude and TC frequency in
233 TC seasons over 1979-2020 for each basin and hemisphere, including (a) NH, (b) NA, (c)
234 WNP, (d) ENP, (e) SH, (f) SIO and (g) SP. The magenta line is the linear regression of points
235 for all years including the La Niña years (blue), El Niño years (red) and neutral years (black).
236 The black line is the linear regression from all gray points after the ENSO effect has been
237 removed. The linear regression slope (*m*) and Pearson correlation coefficient (*r*) are also
238 displayed, and they are in bold if they are significant at the 95% significance level.

239

240 the NA, WNP and in the NH as a whole. As the ITCZ position shifts one degree northward,
241 the TCG frequency increases by about 5 and 2 in the NA and WNP, respectively. The ITCZ-
242 TCG correlation is mainly from SIO in SH basins, but it is weak and only significant at the

90% significance level in the SH. There are no significant correlations between the ITCZ position and TCG frequency in the ENP, SIO and SP.

To rule out the ENSO effect on the ITCZ-TCG relationship, the ENSO influence on the ITCZ position has been investigated. Figure 3 shows significant correlations between the ONI and the detrended ITCZ latitude in all basins and hemispheres. The ITCZ is significantly further equatorward for a more positive ONI both globally and in each basin, except in WNP. The negative correlations in the ENP and NA are likely due to the weakening of the meridional SST gradient, the trade winds and the vertical velocity for more positive ONI (Chiang et al. 2002; Alexander et al. 2012; Sasaki et al. 2015; Fu et al. 2017). The correlation between ONI and the detrended TCG frequency is significant in the NA, ENP and SIO (Figure S8). There are fewer TCs in JAS over NA during El Niño (Figure S8b), related to the stronger vertical wind shear (Gray 1984; Latif et al. 2007; Shaman et al. 2009). During El Niño, the fewer TCG in SIO (Figure S8f) may be caused by the suppressed TC activity east of 75°E, which is related to the vorticity, relative humidity and wind shear changes (Ho et al. 2006; Kuleshov et al. 2009; Lin et al. 2020). As for ENP, there are more TCG from 140°W to 112°W during El Niño (Ralph and Gough, 2009; Jien et al. 2015), which may be caused by the reduced wind shear and stronger vertical motion (Camargo et al. 2007; Fu et al. 2017; Chen et al. 2021). In the WNP, the ONI is not correlated with the basin-scale TCG frequency, which could be caused by the more TCG in the eastern part and less in the western part of the WNP during El Niño years, with the eastward shift of the ITCZ (monsoon trough) (Teng et al. 2014). The correlation between ONI and the detrended TCG latitude is also plotted in Figure S9 for reference.

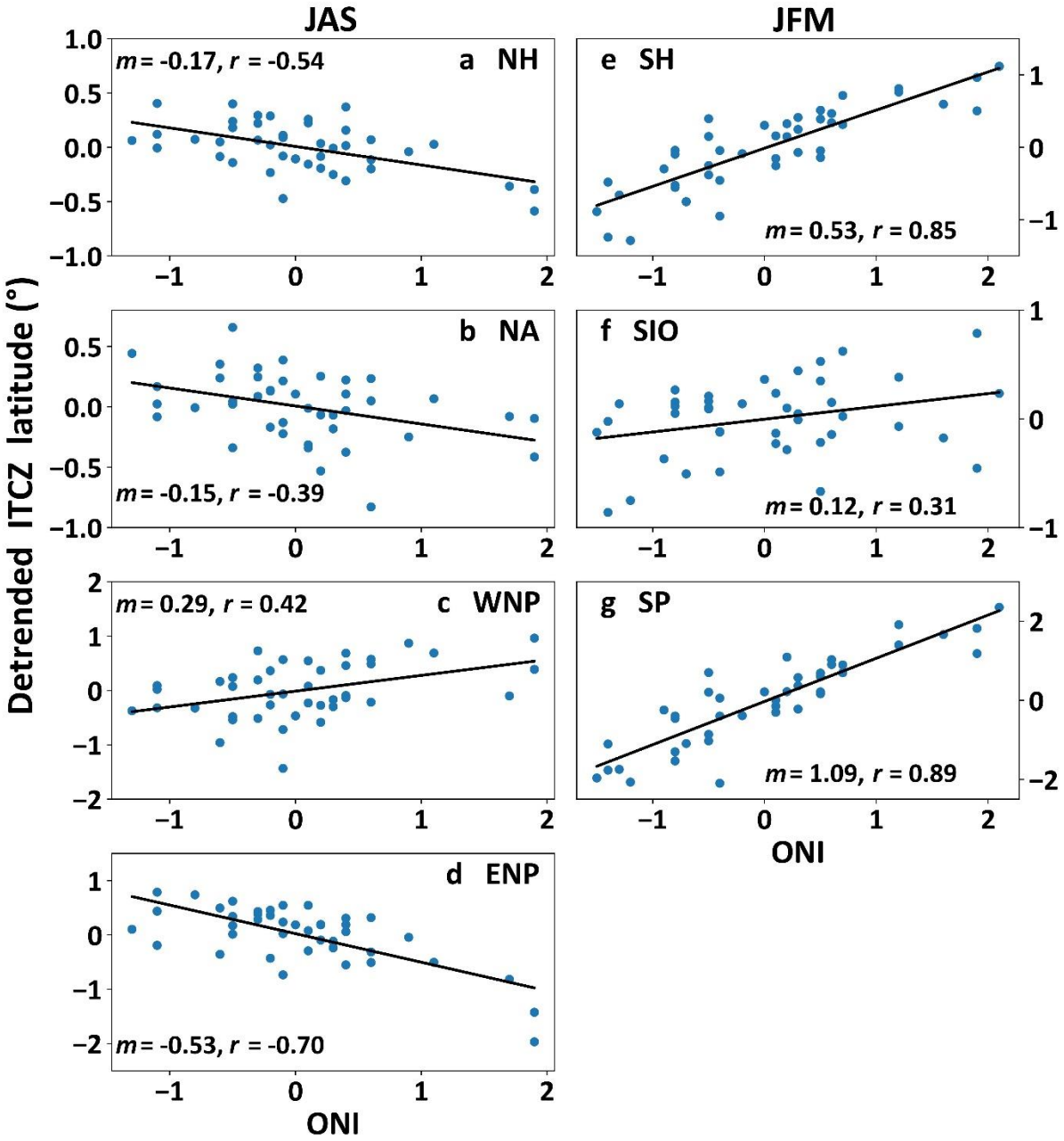

Figure 3. The correlation between ONI and the detrended ITCZ position in TC seasons over 1979-2020 for each basin and hemisphere, including (a) NH, (b) NA, (c) WNP, (d) ENP, (e) SH, (f) SIO and (g) SP. The ONI index and TC season is from July to September (JAS) for basins in the NH and from January to March (JFM) for basins in the SH. The linear regression slopes (*m*) and Pearson correlation coefficients (*r*) in bold are significant at 95% significance level. Please note that the negative latitude anomaly in SH means poleward shift.

After the ENSO signal is linearly removed from the ITCZ position and TCG frequency, the correlations and regressions (black lines and numbers in Figure 2) remain significant in the NA, WNP and NH. Therefore, although the ENSO has strong influences on both ITCZ position and TC frequency, it has generally little effect on the ITCZ-TCG relationship.

To check the sensitivity of the ITCZ-TCG relationship to the ITCZ position from different definitions and datasets with different spatial resolutions, the time series of the detrended ITCZ position using centroid method from GPCP (both 2.5°×2.5° and 1.0°×1.0°), ERA5, and TRMM are plotted in Figure S10. The variability is consistent with significant high correlations. The time series from the maximum precipitation method are plotted in Figure S11 and the variability range is larger compared with that from the centroid method, but results from both methods have significant high correlations. The correlation coefficients between the ITCZ position and TCG frequency, ITCZ intensity and TCG frequency, as well as the ITCZ position and ITCZ intensity over 1979-2020 and 1998-2019 are listed in Tables S5-S8 for references. The correlations vary with datasets, but they are generally consistent, implying the robustness of our results.

b. Large-scale environmental factor influences

In order to further understand the relationship between ITCZ position and TCG frequency, particularly for the interpretation of the weak correlation, large-scale environmental factors affecting TCs are examined. The detrended ITCZ position in NH and detrended absolute ITCZ position in SH over 1979-2020 is sorted in ascending order. The years with the top 12 values are defined as the poleward years, and the bottom 12 years are defined as equatorward years (Table S4). Average differences of the environmental factors between the poleward and equatorward years reveal the changes of these large-scale environmental factors associated with the shift of ITCZ positions.

1) NORTH ATLANTIC

Unlike in other ocean basins, the latitudinal distribution of TCG has double peaks in the NA (Figure S1c), and the TCG position can reach high latitudes (>20°N) that are far away from the ITCZ location. It is found that the ITCZ-TCG relationship is sensitive to the latitude band of TCG. The NA can be split into the north (NA-N, >20°N) and south (NA-S, 0-20°N) bands. The correlation between the ITCZ position and TCG frequency in NA-S can reach 0.63 and 0.56 before and after the ENSO effect is removed (Figure 4a), respectively. In contrast, the ITCZ and TCG have no significant correlation in NA-N, even after removing the ENSO effect (Figure 4b). This suggests the dominance of NA-S TCs in the basin-wide correlation between ITCZ and the TCG frequency (r=0.52 and 0.42 in Figure 2b).

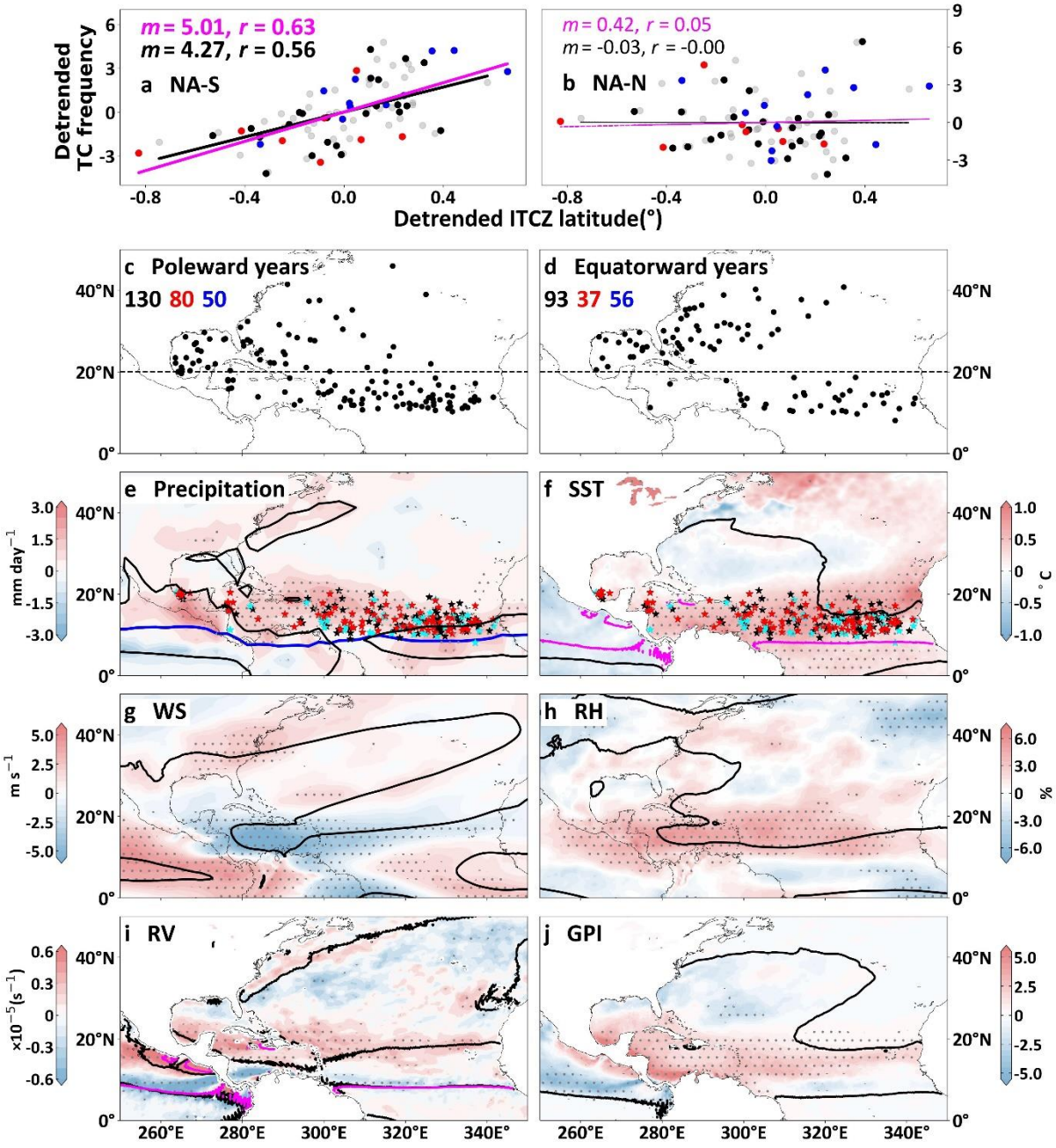

Figure 4. (a-b): As in Figure 3, but for scatter plot between detrended ITCZ latitude and TC frequency in (a) tropical North Atlantic (NA-S), (b) subtropical North Atlantic (NA-N) during 1979-2020. All variables and numbers are calculated over TC seasons. (c) TCG positions in NA during ITCZ poleward years. The black, red and blue numbers in the top left show the numbers of TCG in NA (black), NA-S (0-20°N) (red) and NA-N (>20°N) (blue). (d) As (c), but for ITCZ equatorward years. (e-j) Differences of composited precipitation, SST, vertical wind shear between 200 and 850 h Pa (WS), relative humidity at 600 h Pa (RH), relative vorticity at 850 h Pa (RV) and GPI between the poleward and equatorward years (poleward minus equatorward). Grey stippling indicates significant differences at the 95% confidence level using two-tailed t-test, and black contours represent the climatology of 5 mm day^{-1} (precipitation), 26.5°C (SST), 11 m s^{-1} (WS), 50% (RH), 0 s^{-1} (RV) and 1 (GPI), respectively. RV>0 means anticlockwise rotation and RV＜0 means clockwise rotation in NH. In (e-f), the red, black and cyan stars represent locations of the TCG in NA-S during

ITCZ poleward years, normal years and equatorward years, respectively. The blue line in (e) represents the climatology of the ITCZ position. The magenta contour in (f) and (i) represents the absolute vorticity climatology of $2\times10^{-5}s^{-1}$.

The TCG locations for ITCZ poleward and equatorward years in JAS are shown in Figures 4c, d. There are 130 TCG events in the 12 poleward years, with 80 in NA-S and 50 in NA-N. There are 93 TCs in the 12 equatorward years, with 37 in NA-S (less than half that of poleward years) and 56 in NA-N (similar to that in poleward years). In the ITCZ poleward years, the mean ITCZ position is 9.33°N, while the value in the equatorward years is 8.70°N. The above confirms that in the NA the effect of the ITCZ shift on TC formation is restricted to storms generated in 0°-20°N. The difference of ITCZ positions between poleward and equatorward years is only 0.63° (about 70km), and the TCG frequency difference is 43 in NA-S, which illustrates the strength of the relationship in this region.

The differences (poleward minus equatorward years) in precipitation, SST, vertical wind shear (WS), relative humidity (RH), cyclonic relative vorticity (RV) and the genesis potential index (GPI) are plotted in Figures 4e-j. The TCG locations in the poleward (red star), normal (black star) and equatorward years (cyan star) over the NA-S are also shown in Figures 4e-f. The climatology of the ITCZ position in TC season over 1979-2020 is plotted in Figures 4e-f, showing that TCs all form on the poleward side of this climatological ITCZ. The climatology of other variables is added to Figures 4f-j, such as the contour of 26.5℃ for SST, 11 ms^{-1} for vertical wind shear (McGauley and Nolan 2011), 50% for relative humidity (Cheung 2004), and the absolute vorticity threshold (magenta contour in 4f and 4i) of 2.0×10^{-5} s^{-1} (McGauley and Nolan 2011). In the poleward years, the SST, RH and RV increase over the MDR of the NA-S TCs, and WS decreases. The GPI, which represents the combined effect of the environmental factors (SST, RH, absolute vorticity and WS), has significantly positive anomalies in the MDR in the poleward years as well (Figure 4j). All these environmental factor changes favor TC formation in the tropical NA, and the areas of significant changes in these factors match well with the MDR. These changes are responsible for the close relationship between the ITCZ position and the TCG frequency in the NA-S. The significant warmer SST in NA-S (Figure 4f) caused positive SST anomalies (local minus globally tropical averaged SST) in NA-S and thus reduced the wind shear (Figure 4g, Swanson 2008) and increased the TCG frequency. We also tested the TCG in the area confined by magenta

lines in Figures 1 and S1-S6. This area is generally closer to the ITCZ than the overall TCG area. The results are similar to the current one using the basin-wide TCs.

Some studies also showed the relationship between the African Easterly Waves (AEWs) and the Atlantic TCG (Simpson et al. 1968, 1969; Frank 1970; Thorncroft and Hodges 2001; McCrary et al. 2014) in tropical Atlantic (NA-S), because AEWs are the primary precursor for Atlantic TCG. Russell et al. (2017) pointed out that the correlation between the seasonal mean eddy kinetic energy (EKE) and TCG is maximized in the lower troposphere below the southern AEW storm track, instead of where the canonical AEW is maximized. However, using the convection-permitting regional model simulations, Danso et al. (2022) found that suppressing AEWs did not substantially change seasonal TC frequency, but did influence TC intensity, genesis time and location. For the NA-N, the TCG mechanism may be different from that in NA-S. In subtropics and relatively high latitude regions, TCs could originate from the baroclinic pathways (McTaggart-Cowan et al. 2013), or TCs which originate from tropical waves could migrate and further develop in this region (Mauk and Hobgood 2012). Latest analyses of aquaplanet simulations suggest that subtropical storms complicate (and possibly weaken) the linear relationship between the ITCZ and TC frequency (Zhang et al. 2021). More studies are needed to further understand the combined influences of the ITCZ, AEW and other factors on the TCG.

2) WESTERN NORTH PACIFIC

In WNP, there are 180 TCG events, with 99 in the west (WNP-W, 100-140°E) and 81 in the east (WNP-E, 140-180°E) in the ITCZ poleward years (Figure 5c). Compared to the equatorward years (Figure 5d), there are 8 fewer TCs in the WNP-W and 40 more in the WNP-E, leading to a net increase of 32 TCs in the whole basin from equatorward years to poleward years. The mean ITCZ position is 10.59°N in the poleward years, contrasting with 9.48°N in the equatorward years.

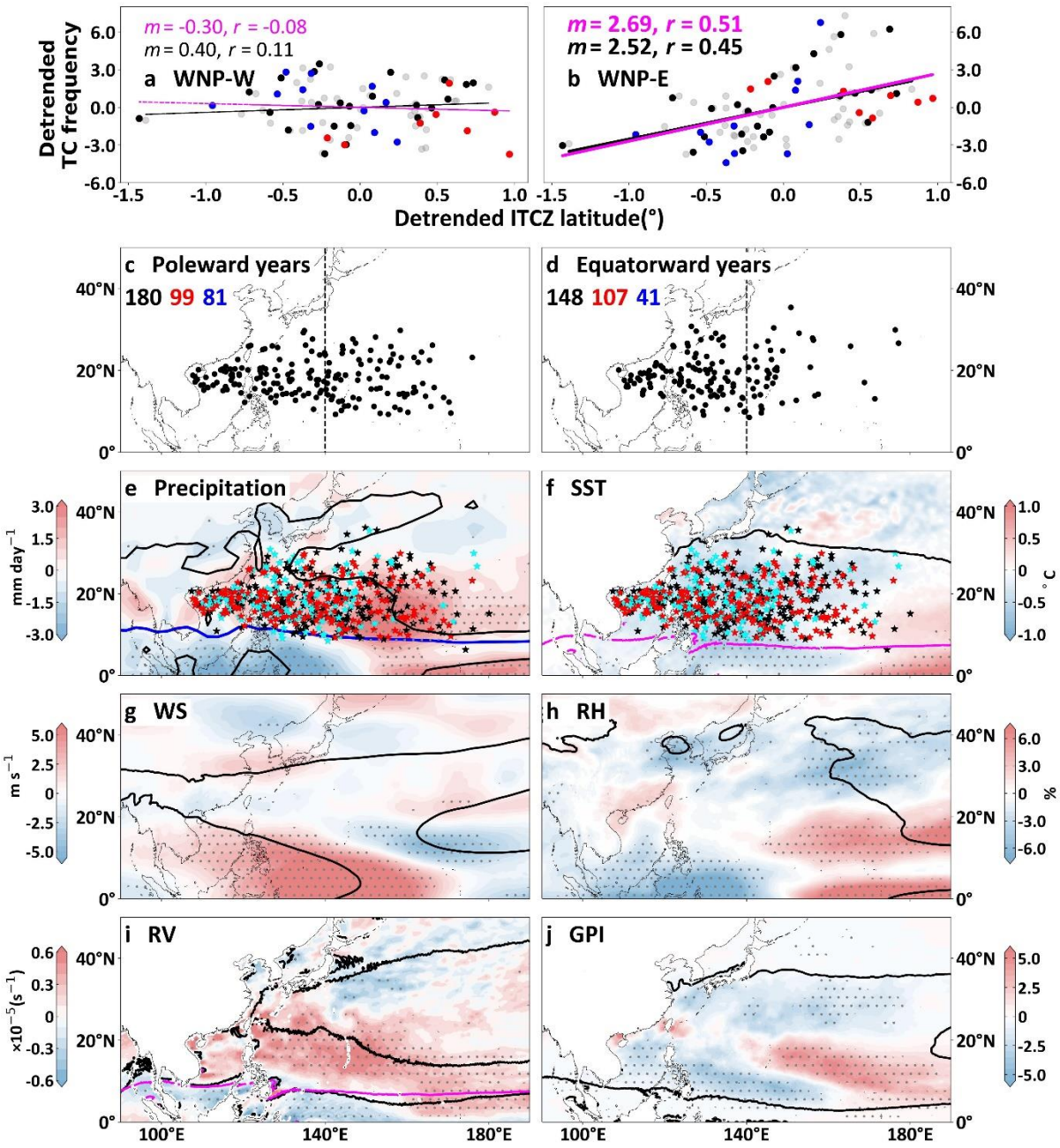

Figure 5. As Figure 4, but for WNP. (a-b): As in Figures 4a-b, but for scatter plot between detrended ITCZ latitude and TC frequency in (a) WNP-W (100-140°E) and (b) WNP-E (140-180°E) in TC seasons during 1979-2020. The 140°E longitude line is marked in (c-d) by the dashed black vertical line. The black, red and blue numbers in (c-d) show the total number of TCG in WNP (black), WNP-W (red) and WNP-E (blue) in TC season.

In the ITCZ poleward years, RV significantly increases in the tropical region and overlaps well with the TC formation area (Figure 5i) in both WNP-E and WNP-W, but the SST and RH significantly reduce in WNP-W and increase in the WNP-E (Figures 5f and h). In these

years, WS significantly increases in the South China Sea and east of the Philippines, where WS is climatologically strong, further inhibiting TC formation (Figure 5g). However, WS significantly reduces in WNP-E (140-180°E, and 10-20°N). GPI further shows a similar pattern with reduction in the west and enhancement in the east. In short, in the ITCZ poleward years, the ITCZ-related environmental changes encourage more TCG events in WNP-E but the effect on the TCG in WNP-W is complicated due to the offsetting changes in environmental conditions. This west-east pattern in the environmental changes corresponds well to the changes in sub-basin TCG frequency. The observed relationship between the ITCZ location and the TCG frequency over the two sub-regions is plotted in Figures 5a-b. Thus, we conclude that the ITCZ-TCG relationship in the WNP is mainly due to the significant environmental changes in the east sector of the basin.

The longitudinal separation of the TCG region in WNP was previously noticed by Chen et al. (1998) and it is attributed to the longitudinal shift of the monsoon trough. Similar separation was also investigated by Wang and Chan (2002), they pointed out that the enhanced tropical storm formation in the southeast quadrant (0^{o}–17^{o}N, 140^{o}E–180^{o}) is attributed to the increase of the low-level shear vorticity generated by El Niño–induced equatorial westerlies, while the suppressed tropical storm generation over the northwest quadrant (17^{o}–30^{o}N, 120^{o}–140^{o}E) is ascribed to upper-level convergence induced by the deepening of the east Asian trough and strengthening of the WNP subtropical high, both resulting from the El Niño forcing. Based on the analysis in this study, the factor contributions to the TCG are complicated and beyond the scope of this paper and need more comprehensive investigations.

3) EASTERN NORTH PACIFIC

Different from NA and WNP, the ITCZ position is weakly correlated with the basin-wide TCG frequency in ENP because of the seesaw changes of large-scale environmental conditions. The decrease of the TCG frequency on the equatorward flank and the increases on the poleward flank cancel each other, leading to small changes in the TCG frequency but large changes in mean TCG latitude. In the ENP, most TCG events concentrate in a small region (10-20°N, 50-90°W, Figures 6a-b), and the ITCZ position is just weakly correlated with the basin-wide TCG frequency (Figure 2d).

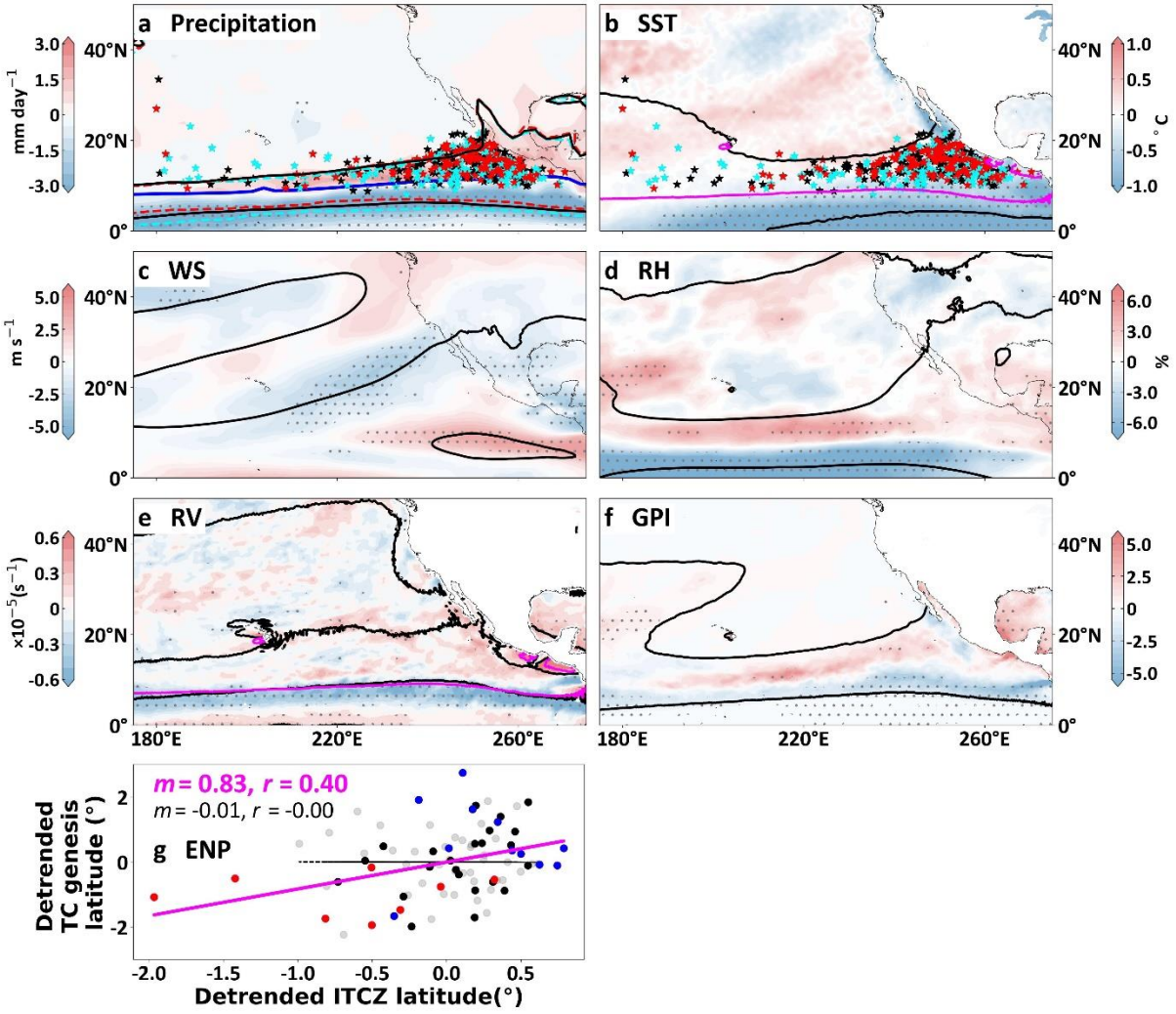

Figure 6. (a-f): As Figures 5e-j, but for Eastern North Pacific. (a) The red and cyan dashed contours are similar to the black contour (the TC season climatology of 5 mm day^{-1} precipitation), but for TC seasons in ITCZ poleward and equatorward years, respectively. (g) As Figure 2d, but for scatter plot of the detrended annual values of ITCZ latitude and TC genesis latitude in TC seasons during 1979-2020.

In the ITCZ poleward years, the associated large-scale environmental conditions exhibit an apparent seesaw change, with warmer SST, weaker WS, higher RH in the north flank of ITCZ, and with colder SST, stronger WS, lower RH and RV in the equatorward flank (Figure 6). The ITCZ shift has a profound effect on the values of environmental conditions especially in the southern part of MDR, as the ITCZ becomes narrower and its southern boundary shifts poleward (in Figure 6a, the southern boundary of the 5mm/day precipitation contours shifts poleward from the cyan one to the black and then the red, which is different from the changes of the northern boundary). The environmental changes favor TCG occurrence in the north and suppress TCG occurrence in the south, and the inhibiting effect in the south is stronger

than the enhancing effect in the north. The favorable genesis region appears to contract in poleward years with the southern part becoming less favorable, leading to the decrease of 20 TCs from equatorward years to poleward years in ENP (from 150 to 130 TCG events).

We further find that ENSO plays a critical role in the relationship between ITCZ position and TCG position in this area. The correlation between ITCZ position and TCG position reaches 0.40 in the ENP, while it decreases to about 0 when ENSO signal is removed (Figure 6g). Both the ITCZ position and TCG position are equatorward in El Niño years (red dots in Figure 6g) and poleward in La Niña years (blue dots in Figure 6g). Except ENSO, the inter-hemispheric temperature difference could also modulate the ITCZ north-south displacement, which could further affect the TCG location (Zhao et al. 2021). The ENP TC formation could be affected by both the ITCZ breakdown (Ferreira and Schubert 1997; Kieu and Zhang 2008; Yokota et al. 2015) and the teleconnections from the NA (Wang and Lee 2009; Wang et al. 2016). To better understand the TCG events in ENP, a further investigation is needed in the future.

4) SOUTH PACIFIC

In the SP, the relationship between the ITCZ position and the TCG frequency is very weak, regardless of whether the ENSO signal is included (Figure 2g). In the ITCZ poleward and equatorward years, the total TCG number is 82 and 85, respectively. In the ITCZ poleward years, the rain belt and the environmental conditions related to TCG significantly shift southward compared with those in the equatorward years (Figures 7a-f).

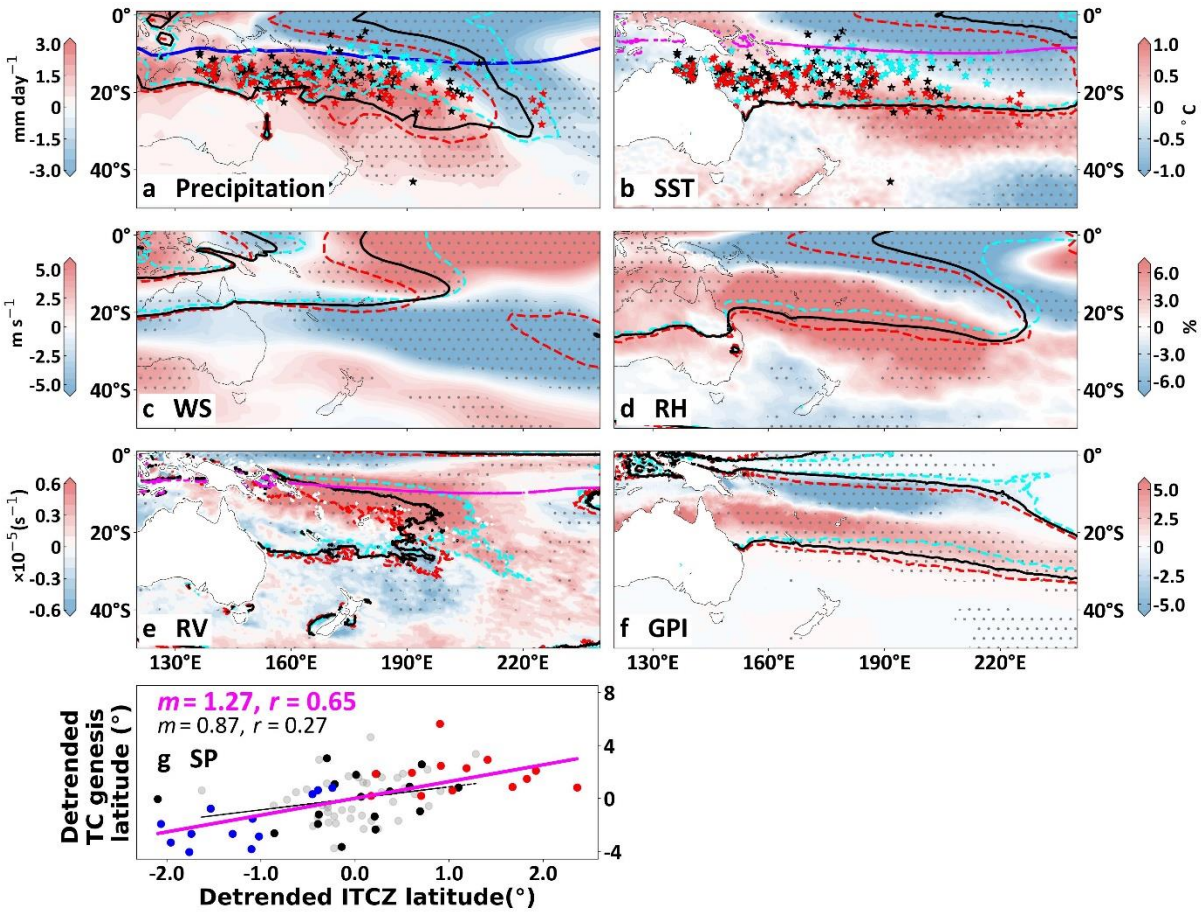

455

456

457 Figure 7. As Figure 6, but for SP. (a-f) The red and cyan dashed contours are similar to
458 the black contour (the TC season climatology), but for TC seasons in ITCZ poleward and
459 equatorward years, respectively. For basins in SH, the blue shade in (e) represents higher
460 cyclonic vorticity. (g) As in Figure 2, but for scatter plot between the detrended ITCZ latitude
461 and TC genesis latitude in TC seasons during 1979-2020. Both the negative ITCZ position
462 and TCG latitude anomalies mean poleward in SH.

463

464 From the poleward to equatorward years, the TCG-associated large-scale environment
465 has significant changes in the tropical region (Figure 7. Note that an increase of cyclonic
466 relative vorticity in the SH is indicated by the negative value). On the equatorward side (0-
467 10°S), there are colder SST, stronger WS, lower RH and lower RV values. In contrast, a large
468 area on the poleward side (10-40°S) sees warmer SST, lower WS, higher RH and higher RV
469 values. The seesaw-like changes in the meridional direction favor TCG occurrence poleward
470 of 20°S but do not favor it equatorward of 20°S (Figure 7f). The GPI change due to ITCZ is
471 constrained to a narrow band (10-30°S). This means that within the climatological position of
472 TCG (alternatively, the MDR), the ITCZ has an apparent compounding effect on the large-

scale environment. This compounding effect can strongly modulate the basin-wide position of TCG events, while it hardly impacts the basin-wide number of TCG events due to the canceling effect in the two sub-regions. As in the ENP, the ITCZ position has strong correlation with the TCG location related partially to the ENSO effect in SP (Figure 7g).

5) SOUTH INDIAN OCEAN

The ITCZ position is weakly correlated with TC frequency in SIO (Figure 2f). The mean ITCZ position is 9.76°S in poleward years and 8.96°S in equatorward years. The total TC number is 115 during poleward years, 20 more than 95 TCs during equatorward years.

The changes in environmental factors over the MDR are mixed in SIO. From the ITCZ poleward years to equatorward years, SST becomes favorable for TCG only in a small area (80-120°E) (Figure 8b). RH becomes favorable for TCG in the most regions of the MDR, except in the west of the basin. WS and RV have neither consistent nor significant changes within the MDR. Consequently, GPI has a weak reduction on the equatorward side of the MDR and a weak increase on the poleward side. This corresponds to the weak ITCZ-TCG correlation over the basin.

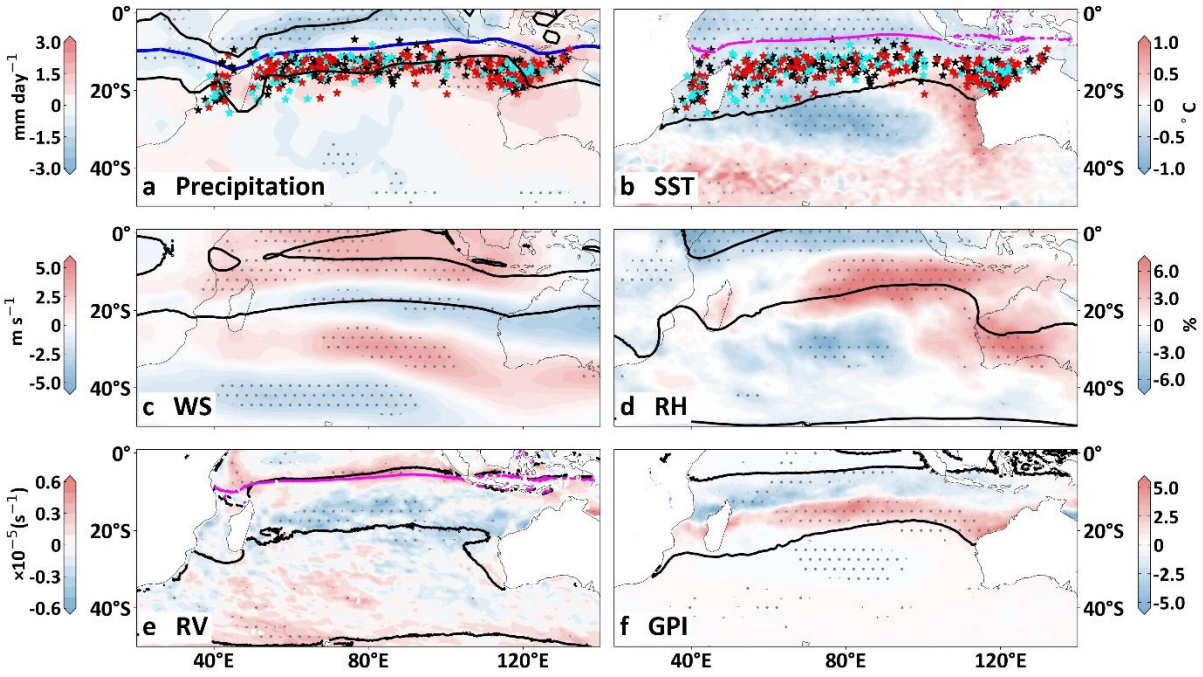

Figure 8. As Figures 7a-f, but for SIO.

4. Summary and Discussion

Previous studies have shown that the TCG frequency is associated with the ITCZ migration in idealized models (Merlis et al. 2013; Ballinger et al. 2015; Burnett et al. 2021; Vu et al. 2021). It is hypothesized that as the ITCZ moves poleward, the subsequent increased Coriolis force and the absolute cyclonic vorticity will favor more TCG events (Ballinger et al. 2015; Burnett et al. 2021). In this paper, we focus on the interannual ITCZ-TCG relationship using the observational data over the last four decades and investigate how the ITCZ modulates the large-scale environment relevant to TCG. Relationships between the ITCZ position and TCG frequency have been examined on the interannual timescale over different basins and hemispheres. The association of this relationship with ITCZ intensity and TCG location is also briefly discussed.

We found that the relationship between the ITCZ position and TCG frequency varies with basins (Figure 2). The ITCZ position is well correlated with the TCG frequency in the NA and WNP. The robust relationship in the NA is from the TCG events in the tropics (0-20N), while the significant relationship in the WNP is due to the TCs formed in the east sector of the basin (140-180°E). A poleward shift of ITCZ in these two basins is associated with significant changes in large-scale environment, which favor TC formation.

In contrast with the NA and WNP, weak correlation is found between ITCZ position and TCG frequency in the ENP, SP and SIO. The environment condition changes relevant to ITCZ have seesaw-like features in the meridional direction both in ENP and SP, with the TC activity suppressed on the equatorward side and enhanced on the poleward side (Figures 6 and 7), leading to the better ITCZ position-TCG location relationship in the ENP and SP. In SP, during ITCZ poleward years, the rain belt and the environmental conditions related to TCG significantly shift poleward compared with those in the equatorward years (Figure 7). In the SIO, the ITCZ-related changes in environmental factors in the MDR are mixed (Figure 8), corresponding to the weak ITCZ position -TCG frequency relationship (Figure 2f).

Although the environmental changes have distinct basin characteristics, there are some similarities across basins between ITCZ poleward and equatorward years. Instead of the Coriolis effect, we focus on the large-scale environment changes modulated by ITCZ movement and its effect on TCG in this study. But the environmental changes related to ITCZ indicate that the Coriolis effect could still play a role. In Figures 4 to 8, the magenta contours in both the relative vorticity (RV) and SST subplots represent the absolute vorticity above the required threshold. Both the climatology regions of the TC formation and cyclonic

relative vorticity changes favorable for TC formation are restricted to the poleward side of the magenta contour, and they are all located at the poleward flank of the rain belt (blue line and black contour in precipitation plot). In addition, as the ITCZ moves poleward, the relative vorticity increases at the high latitude side where there is stronger Coriolis effect, which possibly makes the disturbances associated with ITCZ more likely to occur and makes the vortex more likely to strengthen. These are conducive to the increase of TC frequency, although the increase of vorticity and the amplitude of ITCZ migration vary with basins.

The weak correlation between the ITCZ position and the TCG frequency in the ENP, SP and SIO does not necessarily mean that the ITCZ has a weak effect on TCs in these basins. The ITCZ could impact TCG frequency by different ways and one is by producing disturbances. Previous satellite observations showed that the ITCZ continuously decomposes and produces mesoscale vortices in the central and eastern Pacific, some of which are likely to form TCs (Ferreira and Schubert 1997; Wang and Magnusdottir 2006; Kieu and Zhang 2008). Another way is by providing favorable environment conditions. As shown in Figures 6-8, there are compounding effects and mixed changes in the large-scale environment within the MDR during ITCZ poleward years. Whether the disturbances triggered by the ITCZ could eventually develop into TCs may also be restricted by the environmental conditions, thus affecting the correlation between the ITCZ position and the TC frequency.

This study focuses on the observed relationship between the ITCZ position and the TC frequency over different basins, and environmental changes have been used to interpret the potential processes behind the relationships. This study will help the understanding of the large-scale circulation influences on the TCG at basin-wide and global scales. There are some works worth further research. The changes in environmental factors and GPI may not fully represent the effects of ITCZ migration on TC frequency because they may miss the transient effect on individual TC precursors. Furthermore, the Coriolis parameter never changes at any fixed location, so the effects of poleward ITCZ position are not all directly captured by maps in Figures 4-8. Recent studies (Vecchi et al. 2019; Hsieh et al. 2020; Ikehata and Satoh 2021; Yamada et al. 2021; Yang et al. 2021) showed that the TCG frequency is constrained by the precursor frequency and the survival rate. The poleward movement of ITCZ could contribute to more TCG by increasing precursors (Hsieh et al. 2020), and the survival rate could be restrained by the large-scale environmental factors (Ikehata and Satoh 2021). The influence

of ITCZ position and the large-scale environmental factors on precursor frequency and survival rate need further investigation.

The interaction between the ITCZ position and the TC rainfall is another factor influencing the causal relationship between the TCG number and the ITCZ location. We will investigate this in a separate future study, and it would be an interesting study to remove the effect of TC rainfall on the ITCZ position.

The SST change could also be responsible for the complexity of the ITCZ-TC relationship. A poleward movement of high SST can possibly cause both the poleward ITCZ movement and higher TC frequency. The ITCZ poleward movement that may be nonlinearly driven by SST could further encourage more TCs, increasing the complexity of the ITCZ-TC relationship. Recent studies discussed the effects of climate warming and SST movement on ITCZ location and TC frequency (Merlis et al. 2013; Ballinger et al. 2015; Viale and Merlis 2017; Walsh et al. 2020; Sobel et al. 2021; Zhang et al. 2021). Sensitivity experiments of realistic GCM simulations conditional on ITCZ and SST will help to address this challenge.

Although in our study the correlation coefficients between ITCZ position and TCG frequency have little change after removing ENSO signal, the ENSO effect on the relationship between ITCZ position and TC activity could be complex and nonlinear. During the 12 ITCZ poleward years, there are 5, 6 and 10 La Niña years in NA, ENP and SP, and 6 El Niño years in WNP, respectively. In SIO, there are 5 El Niño years and 4 La Niña years (Table S4). In ENP and SP, the relationships between ITCZ position and TCG latitude changes become obviously weaker after the ENSO signal is removed (Figures 6g and 7g). Pattern changes in large-scale environment between the poleward years and equatorward years in Figures 4-8 resemble those between ENSO years (Kuleshov et al. 2009; Dowdy et al. 2012; Teng et al. 2014; Kim and Moon 2022). These suggest the possible intermediate role of ENSO in regulating the ITCZ-TC relationship, and the ITCZ and ENSO may play a different and nonlinear role in TC activity in different basins.

As shown in Tables S5-S8, the intensity and latitude of ITCZ are correlated and the ITCZ intensity can have a strong correlation with TC frequency in some basins, which is consistent with previous studies (Zhang et al. 2013; Sharmila and Walsh 2018). This is related to the changes of vortices that can subsequently intensify into TCs, resulted from the ITCZ breakdown through the combination of the barotropic instability and the westward-propagating AEWs (Bembenek et al. 2021). Contributions to TCG from the barotropic

instability and AEW have been investigated by Wang and Magnusdottir (2006), Cao et al (2012) and Wu and Takahashi (2018), and the effect of ITCZ instability and monsoon depression on the WNP TCG has also been studied by Beattie et al. (2016). There are other important mechanisms as well about the TCG (Montgomery et al. 2006; Emanuel 2003; Wing et al. 2016). However, detailed studies of these mechanisms are beyond the scope of this study. Besides the ENSO, other climates modes, such as the North Atlantic Oscillation (NAO), Atlantic Meridional Mode (AMM) and Pacific Meridional Mode (PMM) may also play a similar complex role (Hurrel et al. 2003; Frank and Young 2007; Kossin and Vimont 2007; Souza and Cavalcanti 2009; Gao et al. 2018; Murakami et al. 2017; Zhang et al. 2018). The nonlinear processes between ITCZ and TC activity, as well as influences by other climate modes, deserve another study in the future.

Acknowledgments.

This work is jointly supported by the National Natural Science Foundation of China (42275017, 42075036, 72293604, 42130605), Fujian Key Laboratory of Severe Weather (2021KFKT02), the scientific research start-up grant of Guangdong Ocean University (R20001) and the Postgraduate Education Innovation Project of Guangdong Ocean University (202144). Chunlei Liu is also supported by the University of Reading as a visiting fellow. Xiangbo Feng was supported by the UK Met Office Weather and Climate Science for Service Partnership for Southeast Asia, as part of the Newton Fund. We thank three anonymous reviewers for reviewing this paper and providing constructive comments and suggestions.

Data Availability Statement.

The IBTrACS data can be downloaded at https://www.ncei.noaa.gov/products/international-best-track-archive?name=ib-v4-access. The GPCP data are available at https://psl.noaa.gov/data/gridded/data.gpcp.html from National Oceanic and Atmospheric Administration (NOAA) and https://www.ncei.noaa.gov/products/climate-data-records/precipitation-gpcp-daily. The ONI data are from https://origin.cpc.ncep.noaa.gov/products/analysis_monitoring/ensostuff/ONI_v5.php. The ERA5 reanalysis data are downloaded at https://cds.climate.copernicus.eu/cdsapp#!/search?type=dataset.

REFERENCES

Adam, O., T. Bischoff, and T. Schneider, 2016: Seasonal and Interannual Variations of the Energy Flux Equator and ITCZ. Part II: Zonally Varying Shifts of the ITCZ. *J. Climate*, **29**, 7281-7293, https://doi.org/10.1175/jcli-d-15-0710.1.

——, 2016b: Seasonal and Interannual Variations of the Energy Flux Equator and ITCZ. Part II: Zonally Varying Shifts of the ITCZ. *J. Climate*, **29**, 7281-7293, https://doi.org/10.1175/jcli-d-15-0710.1.

Adler, R. F., and Coauthors, 2018: The Global Precipitation Climatology Project (GPCP) Monthly Analysis (New Version 2.3) and a Review of 2017 Global Precipitation. *Atmos.*, **9**, 138, https://doi.org/10.3390/atmos9040138.

——, and Coauthors, 2003: The Version-2 Global Precipitation Climatology Project (GPCP) Monthly Precipitation Analysis (1979–Present). *J. Hydrometeor.*, **4**, 1147-1167, https://doi.org/10.1175/1525-7541(2003)004<1147:TVGPCP>2.0.CO;2.

Alexander, M. A., H. Seo, S. P. Xie, and J. D. Scott, 2012: ENSO's Impact on the Gap Wind Regions of the Eastern Tropical Pacific Ocean. *J. Climate*, **25**, 3549-3565, https://doi.org/10.1175/JCLI-D-11-00320.1.

Ballinger, A. P., T. M. Merlis, I. M. Held, and M. Zhao, 2015: The Sensitivity of Tropical Cyclone Activity to Off-Equatorial Thermal Forcing in Aquaplanet Simulations. *J. Atmos. Sci.*, **72**, 2286-2302, https://doi.org/10.1175/jas-d-14-0284.1.

Beattie, J. C., and R. L. Elsberry, 2016: Western North Pacific monsoon depressions: Transitions to pre-tropical cyclone seedlings. Asia-Pac. *J. Atmos. Sci.*, **52**, 413-435, https://doi.org/10.1007/s13143-016-0025-9.

Bembenek, E., T. M. Merlis, and D. N. Straub, 2021: Influence of Latitude and Moisture Effects on the Barotropic Instability of an Idealized ITCZ. *J. Atmos. Sci.*, **78**, 2677-2689, https://doi.org/10.1175/JAS-D-20-0346.1.

Bischoff, T., and T. Schneider, 2014: Energetic Constraints on the Position of the Intertropical Convergence Zone. *J. Climate*, **27**, 4937-4951, https://doi.org/10.1175/jcli-d-13-00650.1.

Burnett, A. C., A. Sheshadri, L. G. Silvers, and T. Robinson, 2021: Tropical Cyclone Frequency Under Varying SSTs in Aquaplanet Simulations. *Geophys. Res. Lett.*, **48**, e2020GL091980, https://doi.org/10.1029/2020GL091980.

Camargo, S. J., K. A. Emanuel, and A. H. Sobel, 2007: Use of a Genesis Potential Index to Diagnose ENSO Effects on Tropical Cyclone Genesis. *J. Climate*, **20**, 4819-4834, https://doi.org/10.1175/JCLI4282.1.

Cao, X., P. Huang, G. H. Chen, and W. Chen, 2012: Modulation of Western North Pacific tropical cyclone genesis by intraseasonal Oscillation of the ITCZ: A statistical analysis. *Adv. Atmos. Sci.*, **29**, 744–754, https://doi.org/10.1007/s00376-012-1121-0.

Chavas, D. R., and K. A. Reed, 2019: Dynamical Aquaplanet Experiments with Uniform Thermal Forcing: System Dynamics and Implications for Tropical Cyclone Genesis and Size. *J. Atmos. Sci.*, **76**, 2257-2274, https://doi.org/10.1175/jas-d-19-0001.1.

Chen, S., H. Zhao, G. B. Raga, and P. J. Klotzbach, 2021: Modulation of North Pacific and North Atlantic Tropical Cyclones by Tropical Transbasin Variability and ENSO during May–October. *J. Climate*, **34**, 2127-2144, https://doi.org/10.1175/jcli-d-19-0866.1.

Chen, T.-C., S.-P. Weng, N. Yamazaki, and S. Kiehne, 1998: Interannual Variation in the Tropical Cyclone Formation over the Western North Pacific. *Mon. Wea. Rev.*, **126**, 1080-1090, https://doi.org/10.1175/1520-0493(1998)126<1080:Ivittc>2.0.Co;2.

Cheung, K. K. W., 2004: Large-Scale Environmental Parameters Associated with Tropical Cyclone Formations in the Western North Pacific. *J. Climate*, **17**, 466-484, https://doi.org/10.1175/1520-0442(2004)017<0466:Lepawt>2.0.Co;2.

Chiang, J. C. H., Y. Kushnir, and A. Giannini, 2002: Deconstructing Atlantic Intertropical Convergence Zone variability: Influence of the local cross-equatorial sea surface temperature gradient and remote forcing from the eastern equatorial Pacific. *J. Geophys. Res.: Atmos.*, **107**, ACL 3-1-ACL 3-19, https://doi.org/10.1029/2000JD000307.

Danso, D. K., C. M. Patricola, and E. Bercos-Hickey, 2022: Influence of African Easterly Wave Suppression on Atlantic Tropical Cyclone Activity in a Convection-Permitting Model. *Geophys. Res. Lett.*, **49**, e2022GL100590, https://doi.org/10.1029/2022GL100590.

DeMaria, M., J. A. Knaff, and B. H. Connell, 2001: A Tropical Cyclone Genesis Parameter for the Tropical Atlantic. *Wea. Forecast.*, **16**, 219-233, https://doi.org/10.1175/1520-0434(2001)016<0219:Atcgpf>2.0.Co;2.

Donohoe, A., J. Marshall, D. Ferreira, and D. Mcgee, 2013: The Relationship between ITCZ Location and Cross-Equatorial Atmospheric Heat Transport: From the Seasonal Cycle to the Last Glacial Maximum. *J. Climate*, **26**, 3597-3618, https://doi.org/10.1175/jcli-d-12-00467.1.

Dowdy, A. J., L. Qi, D. Jones, H. Ramsay, R. Fawcett, and Y. Kuleshov, 2012: Tropical Cyclone Climatology of the South Pacific Ocean and Its Relationship to El Niño–Southern Oscillation. *J. Climate*, **25**, 6108-6122, https://doi.org/10.1175/jcli-d-11-00647.1.

Emanuel, K., 1991: The theory of hurricanes. Annu. Rev. Fluid Mech., 23, 179-196

——, 2003: Tropical cyclones. Annu. Rev. Earth Planet. Sci., **31**, 75–104, https://doi.org/10.1146/annurev.earth.31.100901.141259.——, 2006: Climate and Tropical Cyclone Activity: A New Model Downscaling Approach. *J. Climate*, **19**, 4797-4802, https://doi.org/10.1175/jcli3908.1.

——, and D. S. Nolan, 2004: Tropical cyclone activity and the global climate system. 26th Conf. on Hurricanes and Tropical Meteorology, Miami, FL, *Amer. Meteor. Soc.*, 240-241, https://ams.confex.com/ams/26HURR/techprogram/paper_75463.htm.

Emanuel, K. A., 1986: An Air-Sea Interaction Theory for Tropical Cyclones. Part I: Steady-State Maintenance. *J. Atmos. Sci.*, **43**, 585-605, https://doi.org/10.1175/1520-0469(1986)043<0585:Aasitf>2.0.Co;2.

Feng, X., N. P. Klingaman, and K. I. Hodges, 2021: Poleward migration of western North Pacific tropical cyclones related to changes in cyclone seasonality. *Nat. Commun.*, **12**, 6210, https://doi.org/10.1038/s41467-021-26369-7.

——, ——, ——, and Y.-P. Guo, 2020a: Western North Pacific Tropical Cyclones in the Met Office Global Seasonal Forecast System: Performance and ENSO Teleconnections. *J. Climate*, **33**, 10489-10504, https://doi.org/10.1175/jcli-d-20-0255.1.

——, Hodges, K. I., Hoang, L., Pura, A. G., Yang, G. Y., Luu, H., ... & Guo, Y. P. (2022b). A new approach to skillful seasonal prediction of Southeast Asia tropical cyclone occurrence. *Journal of Geophysical Research: Atmospheres*, *127*(12), e2022JD036439.

Ferreira, R. N., and W. H. Schubert, 1997: Barotropic Aspects of ITCZ Breakdown. *J. Atmos. Sci.*, **54**, 261-285, https://doi.org/10.1175/1520-0469(1997)054<0261:Baoib>2.0.Co;2.

Frank, N. L., 1970: ATLANTIC TROPICAL SYSTEMS OF 1969. *Mon. Wea. Rev.*, **98**, 307-314, https://doi.org/10.1175/1520-0493(1970)098<0307:ATSO>2.3.CO;2.

Frank, W. M., and G. S. Young, 2007: The Interannual Variability of Tropical Cyclones. *Mon. Wea. Rev.*, **135**, 3587-3598, https://doi.org/10.1175/mwr3435.1.

Frierson, D. M. W., and Y.-T. Hwang, 2012: Extratropical Influence on ITCZ Shifts in Slab Ocean Simulations of Global Warming. *J. Climate*, **25**, 720-733, https://doi.org/10.1175/jcli-d-11-00116.1.

Fu, D., P. Chang, and C. M. Patricola, 2017: Intrabasin Variability of East Pacific Tropical Cyclones During ENSO Regulated by Central American Gap Winds. *Sci. Rep.*, **7**, 1658, https://doi.org/10.1038/s41598-017-01962-3.

Gao, S., L. Zhu, W. Zhang, and Z. Chen, 2018: Strong Modulation of the Pacific Meridional Mode on the Occurrence of Intense Tropical Cyclones over the Western North Pacific. *J. Climate*, **31**, 7739-7749, https://doi.org/10.1175/JCLI-D-17-0833.1.

Gray, W. M., 1968: GLOBAL VIEW OF THE ORIGIN OF TROPICAL DISTURBANCES AND STORMS. *Mon. Wea. Rev.*, **96**, 669-700, https://doi.org/10.1175/1520-0493(1968)096<0669:Gvotoo>2.0.Co;2.

——, 1979: *Hurricanes: Their formation, structure and likely role in the tropical circulation. Meteorology over the Tropical Oceans*, D. B. Shaw, Ed., Royal Meteorological Society, 155–218.

——, 1984: Atlantic Seasonal Hurricane Frequency. Part I: El Niño and 30 mb Quasi-Biennial Oscillation Influences. *Mon. Wea. Rev.*, **112**, 1649-1668, https://doi.org/10.1175/1520-0493(1984)112<1649:Ashfpi>2.0.Co;2.

Hersbach, H., and Coauthors, 2020: The ERA5 global reanalysis. *Quart. J. Roy. Meteor. Soc.*, **146**, 1999-2049, https://doi.org/10.1002/qj.3803.

Ho, C.-H., J.-H. Kim, J.-H. Jeong, H.-S. Kim, and D. Chen, 2006: Variation of tropical cyclone activity in the South Indian Ocean: El Niño–Southern Oscillation and Madden-Julian Oscillation effects. *J. Geophys. Res.: Atmos.*, **111**, D22101 https://doi.org/10.1029/2006JD007289.

Hoogewind, K. A., D. R. Chavas, B. A. Schenkel, and M. E. O'Neill, 2020: Exploring Controls on Tropical Cyclone Count through the Geography of Environmental Favorability. *J. Climate*, **33**, 1725-1745, https://doi.org/10.1175/jcli-d-18-0862.1.

Hsieh, T.-L., G. A. Vecchi, W. Yang, I. M. Held, and S. T. Garner, 2020: Large-scale control on the frequency of tropical cyclones and seeds: a consistent relationship across a hierarchy of global atmospheric models. *Climate Dyn.*, **55**, 3177-3196, https://doi.org/10.1007/s00382-020-05446-5.

Huffman, G. J., and Coauthors, 2007: The TRMM Multisatellite Precipitation Analysis (TMPA): Quasi-Global, Multiyear, Combined-Sensor Precipitation Estimates at Fine Scales. *J. Hydrometeor.*, **8**, 38-55, https://doi.org/10.1175/JHM560.1.

Hurrel, J. W., Y. Kushnir, G. Ottersen, and M. Visbeck, 2003: The North Atlantic Oscillation: climatic significance and environmental impact. American Geophysical Union, 279, 279

Ikehata, K., and M. Satoh, 2021: Climatology of Tropical Cyclone Seed Frequency and Survival Rate in Tropical Cyclones. *Geophys. Res. Lett.*, **48**, e2021GL093626, https://doi.org/10.1029/2021GL093626.

Ivezić, Ž., A. J. Connolly, J. T. VanderPlas, and A. Gray, 2019: *Statistics, data mining, and machine learning in astronomy: A practical python guide for the analysis of survey data*. Princeton University Press, 560 pp.

Jien, J. Y., W. A. Gough, and K. Butler, 2015: The Influence of El Niño–Southern Oscillation on Tropical Cyclone Activity in the Eastern North Pacific Basin. *J. Climate*, **28**, 2459-2474, https://doi.org/10.1175/jcli-d-14-00248.1.

Kieu, C. Q., and D.-L. Zhang, 2008: Genesis of Tropical Storm Eugene (2005) from Merging Vortices Associated with ITCZ Breakdowns. Part I: Observational and Modeling Analyses. *J. Atmos. Sci.*, **65**, 3419-3439, https://doi.org/10.1175/2008jas2605.1.

762 Kim, M.-H., and I.-J. Moon, 2022: Evaluation of the Reliability of Tropical Cyclone Data
763 Using ENSO. Asia-Pac. *J. Atmos. Sci.*, **58**, 365-377, https://doi.org/10.1007/s13143-021-
764 00260-3.

765 Knapp, K. R., M. C. Kruk, D. H. Levinson, H. J. Diamond, and C. J. Neumann, 2010: The
766 International Best Track Archive for Climate Stewardship (IBTrACS): Unifying Tropical
767 Cyclone Data. *Bull. Amer. Meteor. Soc.*, **91**, 363-376,
768 https://doi.org/10.1175/2009bams2755.1.

769 ——, H. J. Diamond, J. P. Kossin, M. C. Kruk, and C. Schreck, 2018: International best track
770 archive for climate stewardship (IBTrACS) project, version 4. NOAA National Centers
771 for Environmental Information.

772 Kossin, J. P., and D. J. Vimont, 2007: A More General Framework for Understanding
773 Atlantic Hurricane Variability and Trends. *Bull. Amer. Meteor. Soc.*, **88**, 1767-1782,
774 https://doi.org/10.1175/bams-88-11-1767.

775 Kuleshov, Y., F. Chane Ming, L. Qi, I. Chouaibou, C. Hoareau, and F. Roux, 2009: Tropical
776 cyclone genesis in the Southern Hemisphere and its relationship with the ENSO. *Ann.*
777 *Geophys.*, **27**, 2523-2538, https://doi.org/10.5194/angeo-27-2523-2009.

778 Latif, M., N. Keenlyside, and J. Bader, 2007: Tropical sea surface temperature, vertical wind
779 shear, and hurricane development. *Geophys. Res. Lett.*, **34**, L01710,
780 https://doi.org/10.1029/2006GL027969.

781 Li, Z., W. Yu, T. Li, V. S. N. Murty, and F. Tangang, 2013: Bimodal Character of Cyclone
782 Climatology in the Bay of Bengal Modulated by Monsoon Seasonal Cycle. *J. Climate*,
783 **26**, 1033-1046, https://doi.org/10.1175/jcli-d-11-00627.1.

784 Lin, I.-I., and Coauthors, 2020: *ENSO and Tropical Cyclones. El Niño Southern Oscillation*
785 *in a Changing Climate*, M.J. McPhaden, A. Santoso and W. Cai, Eds., Amer. Geophys.
786 Union, 377-408, https://doi.org/10.1002/9781119548164.ch17.

787 Liu, C., and Coauthors, 2020: Observed variability of intertropical convergence zone over
788 1998—2018. *Environ. Res. Lett.*, **15**, 104011, https://doi.org/10.1088/1748-9326/aba033.

789 Mauk, R. G., and J. S. Hobgood, 2012: Tropical Cyclone Formation in Environments with
790 Cool SST and High Wind Shear over the Northeastern Atlantic Ocean. *Wea. Forecast.*,
791 **27**, 1433-1448, https://doi.org/10.1175/waf-d-11-00048.1.

McCrary, R. R., D. A. Randall, and C. Stan, 2014: Simulations of the West African Monsoon with a Superparameterized Climate Model. Part II: African Easterly Waves. *J. Climate*, **27**, 8323-8341, https://doi.org/10.1175/JCLI-D-13-00677.1.

McGauley, M. G., and D. S. Nolan, 2011: Measuring Environmental Favorability for Tropical Cyclogenesis by Statistical Analysis of Threshold Parameters. *J. Climate*, **24**, 5968-5997, https://doi.org/10.1175/2011jcli4176.1.

McTaggart-Cowan, R., T. J. Galarneau, L. F. Bosart, R. W. Moore, and O. Martius, 2013: A Global Climatology of Baroclinically Influenced Tropical Cyclogenesis. *Mon. Wea. Rev.*, **141**, 1963-1989, https://doi.org/10.1175/mwr-d-12-00186.1.

Merlis, T. M., and I. M. Held, 2019: Aquaplanet simulations of tropical cyclones. *Curr Climate Change Rep*, **5**, 185-195, https://doi.org/10.1007/s40641-019-00133-y.

——, M. Zhao, and I. M. Held, 2013: The sensitivity of hurricane frequency to ITCZ changes and radiatively forced warming in aquaplanet simulations. *Geophys. Res. Lett.*, **40**, 4109-4114, https://doi.org/10.1002/grl.50680.

Montgomery, M. T., M. E. Nicholls, T. A. Cram, and A. B. Saunders, 2006: A vortical hot tower route to tropical cyclogenesis. *J. Atmos. Sci.*, **63**, 355–386, https://doi.org/10.1175/JAS3604.1.

Murakami, H., and Coauthors, 2017: Dominant Role of Subtropical Pacific Warming in Extreme Eastern Pacific Hurricane Seasons: 2015 and the Future. *J. Climate*, **30**, 243-264, https://doi.org/10.1175/JCLI-D-16-0424.1.

Palmen, E., 1948: On the formation and structure of tropical hurricanes. *Geophysica*, 3, 26-38

Ralph, T. U., and W. A. Gough, 2009: The influence of sea-surface temperatures on Eastern North Pacific tropical cyclone activity. *Theor. Appl. Climatol.*, **95**, 257-264, https://doi.org/10.1007/s00704-008-0004-x.

Ramsay, H. A., S. J. Camargo, and D. Kim, 2012: Cluster analysis of tropical cyclone tracks in the Southern Hemisphere. *Climate Dyn.*, **39**, 897-917, https://doi.org/10.1007/s00382-011-1225-8.

Ritchie, E. A., and G. J. Holland, 1997: Scale Interactions during the Formation of Typhoon Irving. *Mon. Wea. Rev.*, **125**, 1377-1396, https://doi.org/10.1175/1520-0493(1997)125<1377:Sidtfo>2.0.Co;2.

822 Russell, J. O., A. Aiyyer, J. D. White, and W. Hannah, 2017: Revisiting the connection
823 between African easterly waves and Atlantic tropical cyclogenesis. *Geophys. Res. Lett.*,
824 **44**, 587-595, https://doi.org/10.1002/2016GL071236.

825 Sasaki, W., T. Doi, K. J. Richards, and Y. Masumoto, 2015: The influence of ENSO on the
826 equatorial Atlantic precipitation through the Walker circulation in a CGCM. *Climate*
827 *Dyn.*, **44**, 191-202, https://doi.org/10.1007/s00382-014-2133-5.

828 Schmitt, D., E. Gischler, F. S. Anselmetti, and H. Vogel, 2020: Caribbean cyclone activity:
829 an annually-resolved Common Era record. *Sci. Rep.*, **10**, 11780,
830 https://doi.org/10.1038/s41598-020-68633-8.

831 Schneider, T., T. Bischoff, and G. H. Haug, 2014: Migrations and dynamics of the
832 intertropical convergence zone. *Nature*, **513**, 45-53, https://doi.org/10.1038/nature13636.

833 Shaman, J., S. K. Esbensen, and E. D. Maloney, 2009: The Dynamics of the ENSO–Atlantic
834 Hurricane Teleconnection: ENSO-Related Changes to the North African–Asian Jet Affect
835 Atlantic Basin Tropical Cyclogenesis. *J. Climate*, **22**, 2458-2482,
836 https://doi.org/10.1175/2008jcli2360.1.

837 Sharmila, S., and K. J. E. Walsh, 2018: Recent poleward shift of tropical cyclone formation
838 linked to Hadley cell expansion. *Nature Climate Change*, **8**, 730-736,
839 https://doi.org/10.1038/s41558-018-0227-5.

840 Simpson, R. H., N. Frank, D. Shideler, and H. M. Johnson (1968), Atlantic tropical
841 disturbances 1967, *Mon. Weather Rev*., **96**(4), 251–259.

842 Simpson, R. H., N. Frank, D. Shideler, and H. M. Johnson (1969), Atlantic tropical
843 disturbances of 1968, *Mon. Weather Rev.*, **97**, 240–255

844 Sobel, A. H., A. A. Wing, S. J. Camargo, C. M. Patricola, G. A. Vecchi, C.-Y. Lee, and M.
845 K. Tippett, 2021: Tropical Cyclone Frequency. *Earth's Future*, **9**, e2021EF002275,
846 https://doi.org/10.1029/2021EF002275.

847 Souza, P., and I. F. A. Cavalcanti, 2009: Atmospheric centres of action associated with the
848 Atlantic ITCZ position. *Int. J. Climatol.*, **29**, 2091-2105, https://doi.org/10.1002/joc.1823.

849 Swanson, K. L., 2008: Nonlocality of Atlantic tropical cyclone intensities. *Geochem.*
850 *Geophys. Geosyst.*, **9**, https://doi.org/10.1029/2007GC001844.

851 Swapna, P., and Coauthors, 2022: Increasing Frequency of Extremely Severe Cyclonic
852 Storms in the North Indian Ocean by Anthropogenic Warming and Southwest Monsoon
853 Weakening. *Geophys. Res. Lett.*, **49**, e2021GL094650,
854 https://doi.org/10.1029/2021GL094650.

855 Teng, H.-F., C.-S. Lee, and H.-H. Hsu, 2014: Influence of ENSO on formation of tropical
856 cloud clusters and their development into tropical cyclones in the western North Pacific.
857 *Geophys. Res. Lett.*, **41**, 9120-9126, https://doi.org/10.1002/2014GL061823.

858 Thorncroft, C., and K. Hodges, 2001: African Easterly Wave Variability and Its Relationship
859 to Atlantic Tropical Cyclone Activity. *J. Climate*, **14**, 1166-1179,
860 https://doi.org/10.1175/1520-0442(2001)014<1166:Aewvai>2.0.Co;2.

861 Vecchi, G. A., and Coauthors, 2019: Tropical cyclone sensitivities to CO2 doubling: roles of
862 atmospheric resolution, synoptic variability and background climate changes. *Climate*
863 *Dyn.*, **53**, 5999-6033, https://doi.org/10.1007/s00382-019-04913-y.

864 Viale, F., and T. M. Merlis, 2017: Variations in tropical cyclone frequency response to solar
865 and CO2 forcing in aquaplanet simulations. *J. Adv. Model. Earth Syst.*, **9**, 4-18,
866 https://doi.org/10.1002/2016MS000785.

867 Vu, T.-A., C. Kieu, D. Chavas, and Q. Wang, 2021: A Numerical Study of the Global
868 Formation of Tropical Cyclones. *J. Adv. Model. Earth Syst.*, **13**, e2020MS002207,
869 https://doi.org/10.1029/2020MS002207.

870 Walsh, K. J. E., S. Sharmila, M. Thatcher, S. Wales, S. Utembe, and A. Vaughan, 2020: Real
871 World and Tropical Cyclone World. Part II: Sensitivity of Tropical Cyclone Formation to
872 Uniform and Meridionally Varying Sea Surface Temperatures under Aquaplanet
873 Conditions. *J. Climate*, **33**, 1473-1486, https://doi.org/10.1175/jcli-d-19-0079.1.

874 Wang, B., and J. C. L. Chan, 2002: How Strong ENSO Events Affect Tropical Storm
875 Activity over the Western North Pacific. *J. Climate*, **15**, 1643-1658,
876 https://doi.org/10.1175/1520-0442(2002)015<1643:HSEEAT>2.0.CO;2.

877 Wang, C.-c., and G. Magnusdottir, 2006: The ITCZ in the Central and Eastern Pacific on
878 Synoptic Time Scales. *Mon. Wea. Rev.*, **134**, 1405-1421,
879 https://doi.org/10.1175/mwr3130.1.

880 Wang, C., and S.-K. Lee, 2009: Co-variability of tropical cyclones in the North Atlantic and
881 the eastern North Pacific. *Geophys. Res. Lett.*, **36**, L24702,
882 https://doi.org/10.1029/2009GL041469.

883 ——, L. Wang, X. Wang, D. Wang, and L. Wu, 2016: North-south variations of tropical
884 storm genesis locations in the Western Hemisphere. *Geophys. Res. Lett.*, **43**, 11,367-
885 311,374, https://doi.org/10.1002/2016GL071440.

886 Wang, Q., C. Kieu, and T. A. Vu, 2019: Large-scale dynamics of tropical cyclone formation
887 associated with ITCZ breakdown. *Atmos. Chem. Phys.*, **19**, 8383-8397,
888 https://doi.org/10.5194/acp-19-8383-2019.

889 Wilks, D. S., 2011: *Statistical methods in the atmospheric sciences*. Vol. 100, Academic
890 press.

891 Wing, A. A., S. J. Camargo, and A. H. Sobel, 2016: Role of radiative–convective feedbacks
892 in spontaneous tropical cyclogenesis in idealized numerical simulations. *J. Atmos. Sci.*,
893 **73**, 2633–2642, https://doi.org/10.1175/JAS-D-15-0380.1.

894 Wu, L., and M. Takahashi, 2018: Contributions of tropical waves to tropical cyclone genesis
895 over the western North Pacific. *Climate Dyn.*, **50**, 4635-4649,
896 https://doi.org/10.1007/s00382-017-3895-3.

897 Yamada, Y., and Coauthors, 2021: Evaluation of the contribution of tropical cyclone seeds to
898 changes in tropical cyclone frequency due to global warming in high-resolution multi-
899 model ensemble simulations. *Prog. Earth Planet. Sci.*, **8**, 11,
900 https://doi.org/10.1186/s40645-020-00397-1.

901 Yang, W., T.-L. Hsieh, and G. A. Vecchi, 2021: Hurricane annual cycle controlled by both
902 seeds and genesis probability. *Proc. Natl. Acad. Sci*, **118**, e2108397118,
903 https://doi.org/10.1073/pnas.2108397118.

904 Yokota, S., H. Niino, and W. Yanase, 2015: Tropical Cyclogenesis due to ITCZ Breakdown:
905 Idealized Numerical Experiments and a Case Study of the Event in July 1988. *J. Atmos.*
906 *Sci.*, **72**, 3663-3684, https://doi.org/10.1175/jas-d-14-0328.1.

907 Zhang, G., and Z. Wang, 2013: Interannual Variability of the Atlantic Hadley Circulation in
908 Boreal Summer and Its Impacts on Tropical Cyclone Activity. *J. Climate*, **26**, 8529-8544,
909 https://doi.org/10.1175/jcli-d-12-00802.1.

910 Zhang, G., L. G. Silvers, M. Zhao, and T. R. Knutson, 2021: Idealized aquaplanet simulations
911 of tropical cyclone activity: significance of temperature gradients, hadley circulation, and
912 zonal asymmetry. *J. Atmos. Sci.*, **78**, 877-902, https://doi.org/10.1175/JAS-D-20-0079.1.

913 Zhang, W., G. Villarini, G. A. Vecchi, and H. Murakami, 2018: Impacts of the Pacific
914 Meridional Mode on Landfalling North Atlantic tropical cyclones. *Climate Dyn.*, **50**, 991-
915 1006, https://doi.org/10.1007/s00382-017-3656-3.

916 Zhao, H., and C. Wang, 2019: On the relationship between ENSO and tropical cyclones in
917 the western North Pacific during the boreal summer. *Climate Dyn.*, **52**, 275-288,
918 https://doi.org/10.1007/s00382-018-4136-0.

919 ——, R. Yoshida, and G. B. Raga, 2015: Impact of the Madden–Julian Oscillation on
920 Western North Pacific Tropical Cyclogenesis Associated with Large-Scale Patterns. *J.*
921 *Appl. Meteor. Climatol.*, **54**, 1413-1429, https://doi.org/10.1175/jamc-d-14-0254.1.

922 ——, K. Zhao, J. Cao, P. J. Klotzbach, G. B. Raga, and Z. Ma, 2021: Meridional Migration
923 of Eastern North Pacific Tropical Cyclogenesis: Joint Contribution of Interhemispheric
924 Temperature Differential and ENSO. *J. Geophys. Res.: Atmos.*, **126**, e2020JD034504,
925 https://doi.org/10.1029/2020JD034504.

926